QoS-Driven UAVs Placement Optimization and Bandwidth Allocation in Mixed FSO/RF Systems with OIRS Integration

Phong D. Pham, Thang V. Nguyen, Dung D. Tran, Hien T. T. Pham, and Ngoc T. Dang, *Senior Member, IEEE*,

***Abstract*—This paper addresses the problem of ensuring high-capacity, reliable wireless connectivity in temporary or disaster-stricken urban environments. We propose an optical intelligent reflecting surface (OIRS)-enhanced free-space optical (FSO) backhaul framework integrated with unmanned aerial vehicles (UAVs) to overcome the limitations of conventional FSO systems, such as line-of-sight (LOS) blockages. Specifically, OIRS deployed on high-rise buildings intelligently redirects optical beams, creating virtual LOS paths and stabilizing FSO links between the ground station and UAVs. To fully exploit this architecture, we develop a comprehensive channel model that accounts for path loss, turbulence-induced fading, and pointing errors, and introduce the OPT-UAV algorithm for joint UAVs 3D placement, user association, and bandwidth allocation under backhaul capacity constraints. Numerical results demonstrate that the proposed framework improves fairness and coverage by serving up to 67% of mobile users, compared to 62% with baseline methods, such as the TLA algorithm, while maintaining competitive throughput. These results confirm the potential of OIRS-assisted mixed FSO/RF systems as a scalable and resilient solution for smart city deployments, disaster recovery, and temporary high-traffic events.**

***Index Terms*—Free-space optics (FSO), optical intelligent reflecting surface (OIRS), and unmanned aerial vehicle (UAV).**

I. Introduction

A. Background and Research Motivation

Recently, the rapid proliferation of data-hungry applications and the increasing demand for ubiquitous wireless connectivity have pushed current wireless infrastructures to their limits, especially in urban environments and during temporary or temporary events. In such scenarios, the ability to rapidly deploy high-capacity, low-latency wireless backhaul links is crucial. Conventional radio frequency (RF)-based solutions face challenges such as limited spectrum availability, high interference, and security concerns. In contrast, free space optical (FSO) communication has emerged as a promising backhaul technology due to its high data rate capability, license-free spectrum, narrow beamwidth, and resistance to electromagnetic interference [1].

However, the inherent requirement for a strict line-of-sight (LOS) path in FSO systems poses a critical limitation, particularly in dense urban areas where buildings, infrastructure, or dynamic obstructions frequently block the optical path [2]. This challenge becomes more pronounced in emergencies where the infrastructure might be damaged or unavailable. To address this, unmanned aerial vehicles (UAVs) have gained traction as flexible mobile aerial relay nodes capable of extending coverage, enhance connection reliability, and provide access in areas where terrestrial infrastructure is difficult to deploy [3]. Nevertheless, channel fading is a significant element influencing the efficacy of UAV-assisted communication systems, especially in metropolitan settings and emergency situations. Owing to the altitude oscillations of UAVs and the existence of intricate obstructions, wireless connections frequently experience composite fading effects, encompassing substantial route loss and minor fluctuations, resulting in considerable discrepancies in link reliability and quality of service. Multiple credible studies have thoroughly examined these effects, revealing that channel fading can lead to elevated outage probability and significant throughput deterioration in UAV networks [4]–[6]. In addition, establishing reliable FSO links between the ground station (GS) and UAVs remains a challenge due to misalignment issues and environmental turbulence. Recent advances in reconfigurable intelligent surfaces (RIS), and specifically their optical counterparts, optical intelligent reflecting surfaces (OIRS), offer new possibilities to mitigate LOS blockages by intelligently redirecting optical signals. By deploying OIRS on building rooftops, blocked FSO

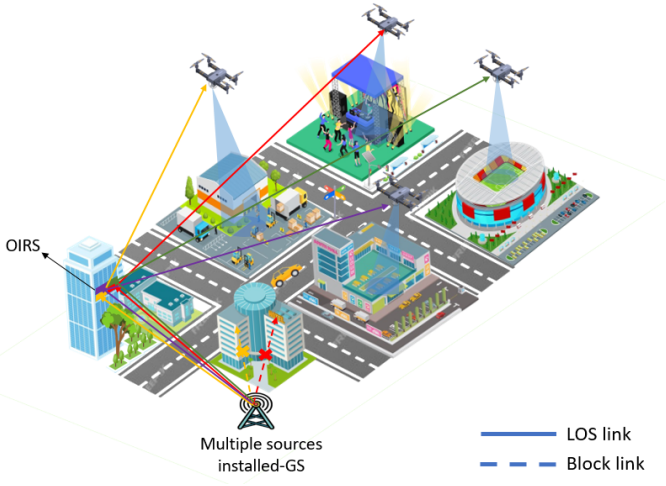

Fig. 1. UAVs deployment to aid mixed FSO/RF systems with OIRS integration.

Phong D. Pham, Thang V. Nguyen, Hien T.T. Pham, and Ngoc T. Dang are with the Wireless Systems and Applications Laboratory, Posts and Telecommunications Institute of Technology, Hanoi 100000, Vietnam. (Corresponding author: Thang V. Nguyen, email: thangnv@ptit.edu.vn).

Dung D. Tran is with the Faculty of Information Technology, University of Transport Technology, Hanoi, Vietnam.

links can be re-established via reflected paths, creating virtual LOS links and improving the availability and robustness of the FSO backhaul [7].

This research is motivated by the need to improve the reliability, flexibility, and efficiency of FSO backhaul systems in complex and dynamic environments. By integrating OIRS into a UAVs-assisted mixed FSO/RF systems, we aim to enable adaptive link formation, minimize link interruptions, and enhance overall network performance. Fig. 1 presents the proposed model for an OIRS-assisted FSO communication system designed for irregular events. In this model, multiple optical sources co-located at a GS transmit FSO signals toward UAVs that act as aerial relays [8], [9]. However, in dense urban environments, direct LOS links between the GS and UAVs are often blocked by buildings and other obstacles. To overcome this limitation, an OIRS is strategically deployed on a high-rise building to redirect optical beams via intelligent reflection, thereby re-establishing LOS connectivity through alternative paths. The UAVs, once connected via robust FSO backhaul links, provide wireless RF access to ground MUs distributed in various hotspot areas such as stadiums, public events, and intersections. This mixed OIRS-enhanced FSO/RF framework offers improved link availability, adaptive deployment, and rapid scalability, which are critical for post-disaster recovery, temporary capacity boosting, and resilient network coverage in complex urban environments.

B. Related Works

A substantial body of research has recently investigated the use of UAVs to enhance mobile access networks and support temporary communications [10]–[15]. In [10], Sun and Ansari explored the deployment of UAVs in high-traffic regions to support content transmission from an GS to an OIRS mounted on a building, which subsequently reflects the optical signal to multiple UAVs acting as aerial base stations to serve MUs, where both UAVs positioning and user association were jointly optimized to improve the spectral efficiency of the area. Similarly, Yaliniz *et al.* [11] investigated optimal altitude and coverage area for a UAV to serve as many MUs as possible while ensuring that the path loss experienced by each associated user remains below a specified threshold to satisfy the quality of service (QoS) constraints. Moving beyond single-UAV scenarios, Zhang *et al.* [12] proposed a 3D deployment strategy that involves multiple UAVs in a given hotspot, aiming to minimize the total number of UAVs required while still meeting the QoS needs of all MUs in the region. Besides, UAVs have also been examined in the context of temporary and disaster recovery. For example, Erdelj *et al.* [13] used UAVs-assisted wireless sensor networks for disaster management, covering phases such as forecasting, damage assessment, and response. In [14], Narang *et al.* designed a UAVs-based multi-hop ad hoc network to restore connectivity in disaster-affected zones by deploying UAVs that relay data between access points and MUs. Their deployment algorithm focused on optimizing UAVs positions to maximize the network's throughput. Furthermore, Hayajneh *et al.* [15] assumed that MUs would naturally cluster in hotspot zones during emergencies and analyzed how UAVs configurations (positioning and transmit power) and UAVs density influence coverage probability and energy efficiency during downlink transmissions. Nevertheless, these studies rely on conventional deployment strategies and do not exploit OIRS to support multi-UAVs scenarios, leaving significant potential for enhancing coverage.

On another front, FSO communication has been recognized for its ability to provide high-speed point-to-point links [16], [17], and recent research has begun to explore the integration of UAVs into FSO systems. Fawaz *et al.* [18] proposed using a UAV as a relay equipped with an FSO transceiver to bridge the connection between an FSO transmitter and receiver, thus mitigating atmospheric attenuation, especially over long distances. The concept of using UAVs-assisted FSO links as part of the fronthaul/backhaul infrastructure of mobile networks has also emerged [19], where geographically distributed base stations connect to nearby UAVs via FSO links. These UAVs then form an aerial ad hoc network based on FSO to relay data between the mobile core and edge base stations. Building on this architecture, Gu *et al.* [20] proposed a dynamic topology reconfiguration scheme to adjust FSO connections among UAVs in response to varying traffic demands, improving network throughput. Najafi *et al.* [21] introduced a mixed RF/FSO model where UAVs use RF for access links to MUs (for example, in sub-6 GHz bands) and FSO for fronthaul links to a central unit. They analyzed geometric loss in FSO links caused by random fluctuations in the position and orientation of the UAVs while hovering. Moreover, OIRS has been acknowledged as efficient mechanisms to improve FSO link performance by alleviating LoS obstructions and broadening coverage. Multiple studies have examined IRS/OIRS-assisted FSO systems in the context of atmospheric turbulence and pointing inaccuracies, assessing metrics such as outage probability and bit error rate, and revealing substantial enhancements in reliability compared to traditional FSO. Numerous studies have suggested multi-hop or relay-based FSO systems, including OIRS to enhance long-distance connection. Furthermore, the optimization problem involving UAV and IRS has been thoroughly examined in RF and high-frequency networks, concentrating on UAVs trajectory, IRS phase shifts, and resource allocation to enhance coverage, performance, and energy efficiency [22], [23]. These studies show that IRS significantly improves UAVs capabilities, especially in urban settings. However, these works generally adopt simplified channel models and do not address the critical problem of optimally placing UAVs when receiving reflected FSO signals via OIRS, which is essential to fully leverage the benefits of intelligent reflection in complex urban environments.

Although these previous works have progressed UAVs-enabled networking, the majority concentrate either on placement and coverage optimization or on UAVs-based FSO relaying under simplified conditions. Significant limitation as the relationship between FSO backhaul capacity and downlink quality of service for terrestrial consumers is seldom examined. The identified deficiencies prompt this work, which formulates a complete channel model, integrates OIRS to

alleviate LOS obstructions, and explicitly factors in backhaul limitations for UAVs positioning and bandwidth distribution, thereby guaranteeing QoS-aware service provision in intricate urban settings.

C. Main Contributions

This paper presents a novel OIRS-assisted mixed FSO/RF framework that addresses the critical limitations of existing UAVs-based FSO backhaul networks. In particular, the key contributions are summarized as follows:

- **Realistic and Combined Channel Modeling**: We comprehensively developed the FSO channel model by taking optical crosstalk, geometric misalignment, turbulence-induced fading, weather-dependent path loss, and blockage mitigation via OIRS-reflected paths into account. The RF access link accounts for distance-dependent path loss. This unified modeling of multi-source/multi-region optical crosstalk and standard fading effects provides a more practical and comprehensive system model for OIRS-assisted mixed FSO/RF UAVs communications than existing simplified or interference-free approaches.
- **Impact on Downlink User Allocation**: By improving the reliability and capacity of the FSO backhaul, the OIRS indirectly improves the RF-based service delivery to ground MUs. This relationship is explicitly modeled through a system-level optimization problem, where the UAVs' downlink data rate to MUs is constrained by the total backhaul capacity they receive via the GS–OIRS–UAVs FSO links.
- **UAVs Placement and Bandwidth Allocation Algorithm**: We develop an optimization-based algorithm, called the OPT-UAV algorithm, that allows UAVs placement and bandwidth allocation in the considered system. By integrating this algorithm, we validate its effectiveness not only in optimizing user association and data allocation under the backhaul conditions enabled by OIRS but also compared to the conventional algorithm, a.k.a. traffic load aware, to show its usefulness.

The proposed system is investigated in a dynamic urban scenario with multiple MUs, UAVs, and obstacles. The numerical results show a significant improvement in the achievable data rate and service coverage, validating the benefits of deploying OIRS to improve mixed FSO/RF systems.

The remainder of the paper is constructed as follows. Section II first describes the system model. Section III then presents the channel model. Section IV states the formulation of the problem. The QoS-aware UAVs placement and MU association algorithm are presented in Section V. Section VI shows the numerical results. Finally, the key points of the study are summarized in Section VII.

II. System Model

A. System Description

We assume that the base station has n laser sources, which correspond to n UAVs, respectively. OIRS needs to be divided into n regions to independently control the beams from n sources. For the source i, it transmits the optical signal to the i-th region of the OIRS. The signal is reflected to the i-th UAV by OIRS. The received signal of the i-th UAV can be expressed as [25]

$$y_i = r_i + n_i, \tag{1}$$

where r_i the transmitted signal propagates through the i-th fading channel, specifically from the i-th source to the i-th OIRS element and then to the i-th UAV. The received signal is affected by Gaussian white noise n_i, which has a zero mean and a variance of $\sigma_{g_i}^2$. In this scenario, the source emits four optical beams, while the OIRS is segmented into four elements, each corresponding to a distinct UAVs positioned at different locations. As illustrated in Fig. 2, the optical signal received at UAVs comprises both useful and useless signals. In that, the useful signal includes the (1) signal from source i-th to i-th OIRS-elements to i-th UAVs (see Eq. (2a) and Fig. 2(a)) and the signal from the source i-th to other OIRS elements except UAVs of the region i-th to i-th (see Eq. (2b) and Fig. 2(b)). The useless signal includes (1) the interference from other sources, indicating the region i-th OIRS-element (see Eq. (2c) and Fig. 2(c)), and (2) the interference from other sources, indicating the other OIRS-element except for the region i-th (see Eq. (2d) and Fig. 2(d)). The signal of the i-th UAV in Eq. (1) can be re-written as

$$r_i = s_i^{(a)} + s_i^{(b)} + s_i^{(c)} + s_i^{(d)},$$

$$s_i^{(a)} = h_{s_i o_i} h_{o_i u_i} s_i, \tag{2a}$$

$$s_i^{(b)} = \sum_{j=1, j\neq i}^{N} h_{s_i o_j} h_{o_j u_i} s_i, \tag{2b}$$

$$s_i^{(c)} = \sum_{j=1, j\neq i}^{N} \sum_{p=1, p\neq i}^{N} h_{s_j o_p} h_{o_p u_i} s_j, \tag{2c}$$

$$s_i^{(d)} = \sum_{j=1, j\neq i}^{N} h_{s_j o_i} h_{o_i u_i} s_j, \tag{2d}$$

TABLE I
System Parameter Annotations List

Symbol	Description
I	Set of all available UAVs
J	Set of all MUs
i	Index of UAVs ($i \in I$)
j	Index of MUs ($j \in J$)
c_{ij}	Binary variable to indicate the user association
$x_i^u y_i^u$	Horizontal location of UAV i
x_i^o, y_i^o	Horizontal location of UAV i's associated OIRS
x_j, y_j	Horizontal location of MU j
d_{ij}	Distance between UAV i and MU j
$h(x_i^u, y_i^u)$	Altitude of UAV i if UAV i is over location (x_i^u, y_i^u)
$h^{max}(x_i^u, y_i^u)$	Maximum altitude of a UAV at location (x_i^u, y_i^u)
$h^{min}(x_i^u, y_i^u)$	Minimum altitude of a UAV at location (x_i^u, y_i^u)
η_{ij}	Average pathloss between UAV i and MU j
η^{th}	Average pathloss threshold
h_i^o	Altitude of element OIRS i
r_{ij}	Downloading data rate from UAV i to MU j
r_j^{th}	Downloading data rate requirement of MU j

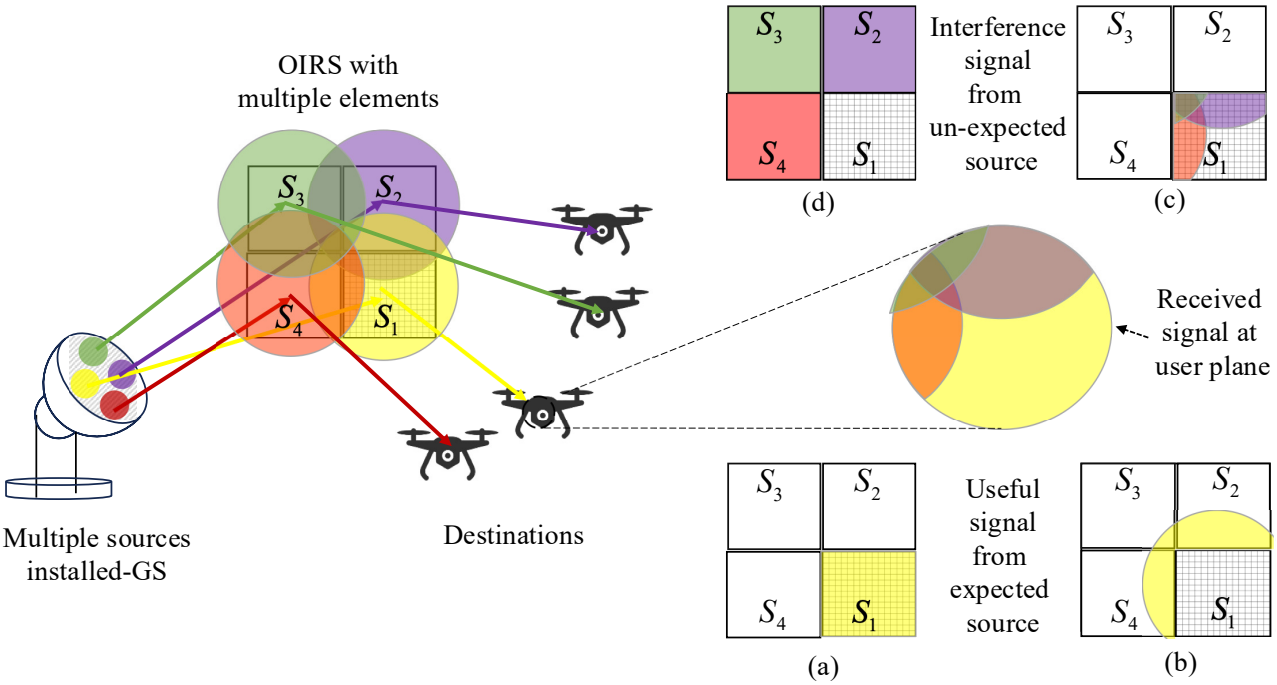

Fig. 2. A description of optical crosstalk in OIRS-aided UAVs communications in irregular events [24].

where s_i is the transmit signal and s_j is the interference source. $h_{s_i o_i}$ and $h_{o_i u_i}$ is the channel coefficient of source-to-OIRS channel and OIRS-to-UAVs channel, respectively.

B. Optical Crosstalk Power

We employ an OIRS, which is divided into four square arrays of equal dimensions. This configuration ensures that each main region is surrounded by three adjacent sections, as depicted in Fig. 2. Given the proximity of the areas within the OIRS and the relatively small size of each region, it is likely that the i-th region will receive signals from other sources. The main source of interference in the primary area arises mostly from beam spillover and the limited aperture of OIRS elements. Beam spillover denotes the escape of optical power from the designated OIRS area to neighboring regions, attributed to Gaussian beam divergence, whereas the finite aperture signifies the constrained physical dimensions of each OIRS component, which intensifies spillover and diminishes reflection efficiency for the intended signal.. Thereby, the primary source of interfering signals in the main region originates mainly from these three neighboring areas. The optical power of the beams concentrated in the i-th region (the main region) and subsequently transmitted to other locations can be expressed mathematically as

$$P_{o_i} = P_i \exp\left(-\frac{d_i^2}{2\omega_L^2}\right), \tag{3}$$

where P_i is the incident light power of i-th region, d_i is the side length of i-th region, and ω_z is the beam waist radius of the incident beam. Similarly, the other overflow optical powers approximating the i-th region can be given as

$$P_{i_{n_t}} = \sum_{m \in M_i} \frac{1}{8} P_m \exp\left(\frac{-d_m^2}{2\omega_z^2}\right), \tag{4}$$

where n_t represents the count of neighboring regions connected to the primary area being examined. The set M_i denotes the neighboring regions connected to the i-th region, while P_m represents the excess power of those neighboring regions. This research examines the overflow power in the regions, assuming that it is identical. This assumption is made based on an estimating expression derived from the region partitioning approach, which allows for a quick estimation of the noise signal strength in nearby regions [25].

C. Model of Average Pathloss Between a UAV and an MU

Communication between MUs and their serving UAVs is usually represented as a probabilistic Line-of-Sight (LoS) channel. The path loss experienced between UAV i and MU j (measured in dB) is denoted as η_{ij}^{LoS} for LoS conditions and η_{ij}^{NLoS} for non-line-of-sight (NLoS) conditions, respectively [26].

$$\eta_{ij}^{LoS} = 20log(\frac{4\pi f_c d_{ij}}{c}) + \xi^{LoS}, \tag{5}$$

$$\eta_{ij}^{NLoS} = 20log(\frac{4\pi f_c d_{ij}}{c}) + \xi^{NLoS}, \tag{6}$$

where f_c is the carrier frequency, c is the speed of light, ξ^{LoS} and ξ^{NLoS} are the average values of excessive path loss in LoS and NLoS, respectively [27].

In addition, d_{ij} represents the distance from UAV i to MU j, is given by $d_{ij} = \sqrt{l_{ij}^2 + h^2(x_i^u, y_i^u)}$ as shown in Fig.

(II-C), where $l_{ij} = \sqrt{(x_i^u - x_j)^2 + (y_i^u - y_j)^2}$ indicates the horizontal distance between UAV i and MU j.

The probability of having LoS connection between UAV i and MU j is given as [27]

$$\rho_{ij} = \frac{1}{1 + be^{-\beta(\theta_{ij} - b)}} \tag{7}$$

where b and β are environment-related constants, θ_{ij} denotes the elevation angle between UAV i and MU i (as described in Fig. (II-C)), is indicated as

$$\theta_{ij} = \arcsin(\frac{h(x_i^u, y_i^u)}{d_{ij}}) \tag{8}$$

We can deduce from Eq. (7) and Eq. (8) that UAV i with a higher altitude results in a larger value of elevation angle, thus triggering a higher probability of having an LoS link.

The average pathloss between UAV i and MU j can be formulated as [28]

$$\bar{\eta_{ij}} = \rho_{ij}\eta_{ij}^{LoS} + (1 - \rho_{ij})\eta_{ij}^{NLoS} \tag{9}$$

Recall that UAV i can link to MU j if the average path loss between UAV i and MU j is less than the specified threshold in advance η^{th}. Thus, the horizontal distance between UAV i and MU j is maximized when

$$\bar{\eta_{ij}} = \eta^{th} \tag{10}$$

Explanation 1: *The optimal elevation angle* (denoted as θ_{ij}^*) between UAV i and MU j is determined as the elevation angle between UAV i and MU j that maximizes the horizontal distance between UAV i and MU j.

The optimal elevation angle θ_{ij}^* between UAV i and MU j can derived from the derivative of η^{th} with respect to θ_{ij} [29]

$$\frac{\pi}{9ln(10)} \tan\theta_{ij}^* + \frac{b\beta(\eta_{ij}^{LoS} + \eta_{ij}^{NLoS})e^{(-\beta(\theta_{ij}^* - b))}}{(be^{(-\beta(\theta_{ij}^* - b)} + 1)^2} = 0 \tag{11}$$

Explanation 2: *The optimal altitude* of the UAV i is determined as the altitude of UAV i that maximizes the horizontal distance between the UAV i and the MU j.

By substituting $\theta_{ij} = \theta_{ij}^*$ into Eq. (10), where θ_{ij}^* is the optimal elevation angle between UAV i and MU j, we can derive the maximum horizontal distance between UAV i and MU j (represented as l_{ij}^{max}). As a result, the optimal altitude of UAV i is given as [29]

$$h_{ij}^* = l_{ij}^{max} \tan\theta_{ij}^* \tag{12}$$

The communication range of UAV i can reach its maximum value if it is deployed at the optimal altitude.

D. Model of RF Access Link

As presented, in temporary networks, multiple UAVs are deployed, each connected to an OIRS installed on a building. The OIRS transmits data traffic to the UAVs, which then relay it to the MUs. To avoid interference, each UAV operates on a separate spectrum band when delivering data to its associated MUs. Let B_i denote the total available bandwidth for the UAV i to serve its MUs. The bandwidth allocated to MU j for downloading data from UAV i is represented by b_{ij}.

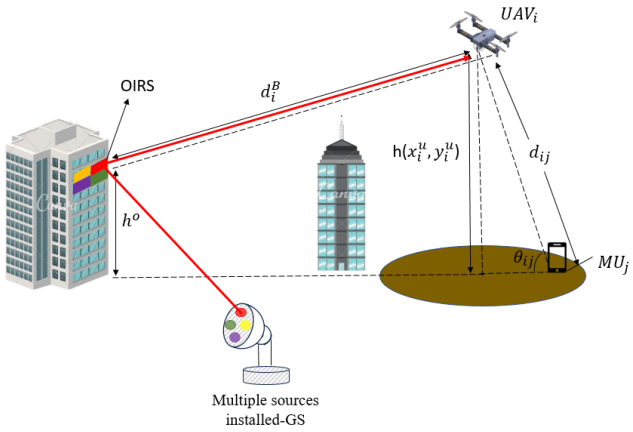

Fig. 3. Path loss model.

Accordingly, the data rate achieved by MU j when receiving traffic from UAV i, denoted as r_{ij}, can be determined

$$r_{ij} = b_{ij}\log(1 + \frac{P_i 10^{\frac{-\bar{\eta_{ij}}}{10}}}{N_0}) \tag{13}$$

where P_i represents the transmission power of UAV i. It is important to note that this work focuses solely on the downlink scenario, as downlink traffic is significantly heavier than uplink traffic [29].

III. Channel Modeling

In an OIRS-assisted multi-UAVs FSO system, the propagation of optical signals is primarily influenced by three factors: path loss, fading caused by atmospheric turbulence, and fading due to pointing misalignment. As a result, the composite channel coefficient h_i is given by [30]

$$h_i = h_{l_i} h_{p_i} h_{a_i} \tag{14}$$

In this expression, h_{l_i} denotes path loss, which varies based on the transmission distance and weather conditions. The factor h_{p_i} represents the power attenuation resulting from the misalignment between the transmitter and receiver, typically modeled as a random variable. Lastly, h_{a_i} describes the fading effect caused by fluctuations in optical beam intensity as it propagates through a turbulent atmosphere.

A. Propagation Loss

In an open-air environment, the optical signal undergoes attenuation while propagating through the atmosphere due to absorption and scattering. The channel loss coefficient can be expressed based on the Beer-Lambert law as

$$h_{l_i} = \exp(-\alpha_{l_i} L), \tag{15}$$

where L denotes the transmission distance over which these effects take place and α_{l_i} represents the atmospheric attenuation coefficient, which depends on weather conditions and can be expressed as

$$\alpha_{l_i} = \frac{3.91}{v}\left(\frac{550}{\lambda}\right)^{-q} \tag{16}$$

where λ represents the optical wavelength, v is the visibility (the maximum distance that one object can be clearly discerned). In addition, the coefficient q as the size distribution of the scattering particles. The relationship between q and v is given by [31]

$$q = \begin{cases} 1.6 & v > 50, \\ 1.3 & 6 < v \leq 50, \\ 0.16v + 0.34 & 1 < v \leq 6, \\ v - 0.5, & 0.5 \leq v \leq 1, \\ 0, & v \leq 0.5 \end{cases} \tag{17}$$

where the value of v depends on the weather conditions. For example,$v > 50$ when weather is a clear sky, $1 < v < 6$ for a hazy weather, and $v \leq 1$ for foggy weather [31].

B. Atmospheric Turbulence

Besides path loss, the atmospheric channel also introduces random variations in the transmitted beam intensity, leading to signal fading at the receiver. To facilitate performance analysis, various statistical models have been developed to characterize this turbulence-induced fading. In the case of turbulence operating in moderate and strong regimes, the gamma-gamma distribution is often used to model its characteristics [32]. The gamma–gamma distribution is employed to model atmospheric turbulence because it effectively captures moderate-to-strong effects, which are commonly encountered in terrestrial networks (TN) and non-terrestrial networks (NTN) [33], [34]. The parameters α and β in Eq. (19) and Eq. (20) are selected to correspond to moderate turbulence conditions that are prevalent in many practical TN and NTN deployments. Although these parameter choices may lead to somewhat optimistic estimates in extreme weather conditions (e.g., heavy fog or sandstorms with significantly higher attenuation), they provide a representative and widely accepted basis for performance evaluation under typical operating conditions of UAVs-based mixed FSO/RF communication systems. Hence, the PDF of the turbulence-induced fading h_{a_i} can be written as [35]

$$f_{h_{a_i}}(h_{a_i}) = \frac{2(\alpha\beta)^{(\alpha+\beta)/2}}{\Gamma(\alpha)\Gamma(\beta)} h_{a_i}^{\frac{\alpha+\beta}{2}-1} \mathrm{K}_{\alpha-\beta}(2\sqrt{\alpha\beta h_{a_i}}), \tag{18}$$

where $\mathrm{K}_{\alpha-\beta}(.)$ is the modified Bessel function of the second kind and order (α-β) and $\Gamma(\cdot)$ denotes the gamma function. α and β are the effective numbers of large-scale and small-scale turbulence. In the case of zero inner scale, they are given by

$$\alpha = \left[\exp\left(\frac{0.49\sigma_R^2}{\left(1 + 1.11\sigma_R^{12/5}\right)^{7/6}} \right) - 1 \right]^{-1}, \tag{19}$$

$$\beta = \left[\exp\left(\frac{0.51\sigma_R^2}{\left(1 + 0.69\sigma_R^{12/5}\right)^{5/6}} \right) - 1 \right]^{-1}. \tag{20}$$

C. Misalignment-Induced Fading

In FSO communication, misalignment-induced fading arises from beam misalignment due to mechanical vibrations or device misalignment. This effect is critical in OIRS-assisted systems, where beam deviations impact reflection efficiency and overall signal quality. Based on the physical model of the OIRS jitter, the PDF of jitter angle at the receiving plane can be written as [36]

$$f_{\theta_{u_i}}(\theta_{u_i}) = \frac{\theta_{u_i}}{(1 + L_{R_i})^2 \sigma_{\theta_{u_i}}^2 + 4\sigma_\phi^2} e^{\frac{-\theta_{u_i}^2}{2\left(1+L_{R_i}\right)^2 \sigma_{\theta_{u_i}}^2 + 8\sigma_\phi^2}}, \tag{21}$$

the ratio $L_{R_i} = L_{s_i o_i}/L_{o_i u_i}$ represents the proportion of the distance between the source i-th to OIRS region, denoted as i-th, $L_{s_i o_i}$, and the distance between OIRS region i-th and the receiver i-th, $L_{o_i u_i}$. $\theta \sim \mathcal{N}(0, \sigma_\theta^2)$ and $\phi \sim \mathcal{N}(0, \sigma_\phi^2)$ are the pointing error angle at the transmitter and the deflection angle at the OIRS, respectively. Since θ_{u_i} is the angle corresponding to the optical beam offset in the receiver plane r_i, the instantaneous displacement from the receiver center to the receiving light spot can be determined as

$$r_i = \tan(\theta_{u_i}) L_{o_i u_i} \approx \theta_{u_i} L_{o_i u_i}, \tag{22}$$

Due to the vibration of the building, where mounts OIRS is mounted, the pointing error h_{p_i} can be estimated as

$$h_{p_i} = A_0 \exp\left(-\frac{2r_i^2}{w_{Leq}^2} \right), \tag{23}$$

where $A_0 = [\mathrm{erf}(v)]^2$ is the fraction of the collected power at $r_i = 0$ and $w_{Leq}^2 = w_L^2 \frac{\sqrt{\pi}\mathrm{erf}(v)}{2v\exp(-v^2)}$ is the equivalent beam width in which $v = \sqrt{\frac{\pi}{2}}\frac{a}{w_L}$ is the ratio between aperture radius and the beam width and $w_L = (2\lambda)/(\pi\theta_T)$ is the beam waist radius in which θ_T is the divergence angle.

By substituting (22), (23) into (21) and applying some manipulations, the PDF of h_{p_i} can be given as

$$f_{h_{p_i}}(h_{p_i}) = \frac{w_{Leq}^2}{4A_0\left(\sigma_\theta^2 L_{T,i}^2 + 4\sigma_\beta^2 L_{s_i o_i}^2\right)} \left(\frac{h_{p_i}}{A_0}\right)^{\frac{w_{Leq}^2}{4\sigma_\theta^2 L_{T,i}^2 + 16\sigma_\beta^2 L_{s_i o_i}^2}}. \tag{24}$$

D. Combined Channel Model

The combined channel is developed by considering the comprehensive effect of environmental conditions including propagation loss, pointing misalignment, and fading caused by atmospheric turbulence. From (15), (18), and (24), the PDF of the channel coefficient as

$$f_{h_i}(h_i) = \frac{\alpha\beta\xi^2}{A_0 h_l \Gamma(\alpha)\Gamma(\beta)} \mathrm{G}_{1,3}^{3,0}\left[\frac{\alpha\beta h}{A_0 h_l} \middle| \begin{matrix} \xi^2 \\ \xi^2 - 1, \alpha - 1, \beta - 1 \end{matrix} \right], \tag{25}$$

where $\mathrm{G}_{\mathrm{p,q}}^{\mathrm{m,n}}[\cdot|\cdot]$ denotes the Meijer G-function [24].

IV. Problem Formulation

Assume that the number of available UAVs is predetermined. These UAVs will be deployed to help the MUs in the temporary networks download data from GS reflected via OIRS. Denote c_{ij} as the binary variable to indicate whether MU j is associated with UAV i (i.e., $c_{ij} = 1$) or not

(i.e., $c_{ij} = 0$). We formulate the UAVs configuration and MUs association problem to determine the 3-D locations of UAVs, MUs association, as well as the bandwidth allocation to different MUs in order to maximize the number of satisfied MUs (i.e., their QoS in terms of data rate requirements is met). That is given as [29]:

$$\mathbf{P0}: \arg \max_{x_i^u, y_i^u, h(x_i^u, y_i^u), c_{ij}} \sum_{i \in I} \sum_{j \in J} c_{ij}, \tag{26}$$

$$\text{s.t.:} \quad C1: \sum_{i \in I} c_{ij} \leq 1, \quad \forall j \in J, \tag{27}$$

$$C2: h^{\min}(x_i^u, y_i^u) \leq h(x_i^u, y_i^u) \leq h^{\max}(x_i^u, y_i^u), \tag{28}$$

$$C3: c_{ij}(\eta_{ij} - \eta_{ij}^{th}) \leq 0, \quad \forall j \in J, \forall i \in I, \tag{29}$$

$$C4: c_{ij}(r_{ij} - r_j^{th}) \geq 0, \quad \forall i \in I, \forall j \in J, \tag{30}$$

$$C5: \sum_{j \in J} c_{ij} r_{ij} \leq R_i, \quad \forall i \in I, \tag{31}$$

$$C6: \sum_{j \in J} c_{ij} b_{ij} \leq B_i, \quad \forall i \in I. \tag{32}$$

where constraint C1 ensures that each MU is served by at most one UAV; constraint C2 imposes the altitude constraints of deploying a UAV, where $h^{min}(x_i^u, y_i^u)$ implies the minimum altitude of UAV i to maintain the LoS between UAV i and its communicated OIRS if UAV i is deployed at (x_i^u, y_i^u), $h^{max}(x_i^u, y_i^u)$is the maximum altitude that UAV i can reach. Constraint C3 indicates that MUs j can be link to UAV i (i.e., $c_{ij} = 1$) if the path loss between MUs j and UAV i is not larger than the threshold η^{th} (i.e., $\eta_{ij} - \eta^{th} \leq 0$). Constraint C4 implies that QoS in terms of the data rate requirement of MUs j (denoted as r_j^{th}) should be satisfied if it is associated with UAV i; Constraint C5 implies that the data rate of the backhaul link between UAV i and its associated OIRS should be no less than the data rate of the access link for UAV i (which is equal to the sum of all the data rates of the MUs associated with UAV i). Essentially, Constraint C5 ensures that the backhaul link is not the bottleneck. Constraint C6 ensures the total bandwidth allocated to MUs by each UAV is within the total bandwidth it can use.

In constraint C5, the FSO backhaul rate R_i of UAV i plays a critical role in maintaining the UAVs' ability to serve ground users. A key focus in our study is to explicitly consider the impact of the transmission channel conditions on R_i, rather than assuming it to be a fixed or ideal value. The reliability and capacity of the FSO backhaul link can be severely affected by channel impairments such as atmospheric turbulence, building blockage, and dynamic urban environments. To address these challenges, this work incorporates OIRS into the system model, as shown in Fig. 1. OIRS are strategically deployed on building facades to enhance the quality of the FSO link by intelligently reflecting and redirecting optical signals, mitigating the impact of channel degradation. We utilize the OIRS as an effective solution to adapt to urban obstacles and atmospheric fluctuations dynamically. Through the support of OIRS, the effective FSO backhaul rate R_i is significantly stabilized and improved, ensuring that UAVs maintain consistent connectivity with the network infrastructure. This enhancement is essential for meeting the bandwidth requirements of associated users and sustaining the network performance under the dense and complex conditions of urban temporary scenarios.

Specifically, the average data rate R_i of UAV i is determined based on the following expression

$$\overline{R}_i = \int_0^\infty B_i \log_2(1 + \gamma_i) f_{\gamma_i}(\gamma_i)\, d\gamma_i \tag{33}$$

where B_i is the available bandwidth for each UAV i. $f_{\gamma_i}(\gamma_i)$ is the PDF of γ_i in which γ_i is the instantaneous SNR of UAV i-th the SNR γ_i is given as [25]

$$\gamma_i = \frac{2P_i^2 h_i^2}{2 \sum\limits_{j=1, j \neq i}^{N} h_i^2 P_j^2 + \sigma_{g_i}^2}, \tag{34}$$

where P_j is the transmit power from other sources reflected to the i-th UAV. By using the variable transformation method and averaging over the fading channel created in Eq. (25), the PDF of the instantaneous SNR, which depends on the combined channel, is given as [24]

$$f_{\gamma_i}^{GG}(\gamma_i) = \frac{P_t^2 \xi^2}{\gamma_i \left(2P_t^2 - 2\gamma_i \sum\limits_{j=1, j \neq i}^{N} P_j^2 \right) \Gamma(\alpha)\Gamma(\beta)} \times G_{1,3}^{3,0}\left(\frac{\alpha\beta}{A_0 h_l} \sqrt{\frac{\gamma_i \sigma_{g_i}^2}{2P_t^2 - 2\gamma_i \sum\limits_{j=1, j \neq i}^{N} P_j^2}} \middle| \begin{matrix} \xi^2 \\ \xi^2 + 1, \alpha, \beta \end{matrix} \right). \tag{35}$$

Section III delineates a comprehensive stochastic FSO channel model, whereby the optimization framework does not directly depend on instantaneous fading coefficients to maintain computational feasibility. The channel impact is represented by the average signal-to-noise ratio γ_i, which reflects the anticipated impacts of route loss, air turbulence, and pointing errors. This ratio is used to calculate the backhaul rate in Eq. (33) and in constraint C5. This method facilitates the modeling of random fading effects by using their average characteristics. The channel model in Section III provides the physical basis for parameterizing γ_i, while the optimization issue addresses UAVs placement and resource allocation based on anticipated channel conditions..

V. QoS-Aware UAVs Placement Optimization

In order to efficiently address problem **P0**, we propose an algorithm, called OPT-UAV, that divides the problem into two smaller parts: UAVs placement and bandwidth allocation. By repeatedly solving these two parts, our proposed method is able to achieve a near-optimal solution to **P0**. The detailed steps of the algorithm are described in Algorithm 1.

A. Initial 3-D UAVs Placement

To efficiently deploy UAVs, we assume that the temporary zone is divided into equal-sized locations, set of these areas is denoted as N. Each UAV i is positioned at a specific location $n \in N$, with its 2D coordinates (x_i^u, y_i^u) corresponding to the center of that location. Instead of connecting directly to a GS (i.e., Ground Station), the UAVs links to an OIRS installed on a high-rise building to support backhaul communications in urban environments where optical signals can be blocked. The goal of initial UAVs placement is to maximize coverage by ensuring that each UAV serves the largest possible number of MUs that are not already connected to other UAVs. Let J_0 represent the set of MUs without an assigned UAV, which means $J_0 = \{j \in J \mid c_{ij} = 0, \forall i \in I\}$. When deploying the first UAV, all MUs belong to J_0. To determine the optimal placement for the UAV i, the following iterative approach is used:

*1) **Selecting a Candidate Location**:* Derived from **Explanation 1**, the UAV i is placed over location n, and its optimal altitude h_i^* is determined based on Eq. (12). If the calculated altitude falls outside the predefined range $[h^{min}(x_i^u, y_i^u), h^{max}(x_i^u, y_i^u)]$, it is adjusted to remain within the limits (satisfy C2 in **P0**).

*2) **Coverage Evaluation**:* The average path loss between the UAV i and each MU in J_0 is computed. If the path loss is below a given threshold η^{th}, the MU is considered covered by the UAV i. The set of covered MUs at location n is denoted as K_{in}, with $|K_{in}|$ representing the number of covered MUs by UAV i.

*3) **Optimal Location Selection**:* The process is repeated for all possible locations, and the location maximizing K_{in} is chosen. Thus, the UAV i is placed in the center of this optimal location (denoted $n^* = \text{argmax}\{|K_{in}||n \in N\}$).

B. Optimizing UAVs Altitude

If UAV i cannot meet the bandwidth requirements of some MUs due to resource limitations, its altitude is adjusted to improve coverage. This is done as follows:

*1) **Step Size Definition**:* After determining the optimal altitude of UAV i is h_i^* from **the initial 3-D placement**, h_i^* adjusted through a value called the step size (denoted as δ). We adopt a fixed step size δ is used to ensures low computational complexity and stable convergence, which are essential in emergency scenarios or complex environments. While adaptive step-size methods could improve convergence in highly dynamic environments, they increase complexity due to additional gradient estimation and tuning. Thus, the fixed step size offers a practical trade-off between performance and implementation simplicity.. The step size δ is incrementally increased within the range $[d_{\min}, d_{\max}]$, where $d_{\min}$ and $d_{\max}$ are the minimum and maximum steps. Starting from $\delta = d_{\min}$.

*2) **Altitude Adjustment**:* The altitude of the UAV i increases or decreases by δ (i.e. $h_i^+ = \min(h_i^* - \delta, h^{max}(x_i^u, y_i^u)$ and $h_i^- = \max(h_i^* - \delta, h^{min}(x_i^u, y_i^u)))$, ensuring it stays within the range of $[h^{min}(x_i^u, y_i^u), h^{max}(x_i^u, y_i^u)]$. The number of MUs that can be successfully associated is recalculated by performing the bandwidth allocation and MU association process again based on the updated altitudes of the UAV i (i.e., h_i^- and h_i^+).

*3) **Updating Altitude**:* Define $M(h_i^*), M(h_i^+), M(h_i^-)$ as the number of associated MUs when the altitude of UAV i is h_i^*, h_i^+, and h_i^-, respectively.

- If the adjusted altitude does not increase the number of associated MUs, keep the original altitude h_i^* and update the step size as:

$$\delta = \delta + d_{\min} \tag{36}$$

- If the adjustment increases the number of associated MUs, update the altitude as follows:

$$h_i^* = \begin{cases} h_i^+, & \text{if } M(h_i^+) > M(h_i^*) \text{ and } M(h_i^+) \geq M(h_i^-) \\ h_i^-, & \text{if } M(h_i^-) > M(h_i^*) \text{ and } M(h_i^-) > M(h_i^+) \end{cases} \tag{37}$$

Then, reset the step size to $\delta = d_{\min}$.

*4) **Continue Adjustments**:* Subsequently, we will return to Step 2 and continue adjusting the altitude till $\delta > d_{\max}$.

The proposed approach executes regular changes of UAVs locations, bandwidth allocation, and MU associations to accommodate fluctuations in MU distribution. In the analyzed situations, MUs are assumed to remain quasi-static throughout each optimization period, hence providing steady MU

Algorithm 1 UAVs Placement Optimization and Bandwidth Allocation

```
Partition temporary zone into N equal-sized locations
for each UAV i ∈ I do
    for each location n ∈ N do
        Place UAV i over location n
        Calculate optimal altitude h_n using h^min(x_i^u, y_i^u), h^max(x_i^u, y_i^u)
        Calculate covered MUs |K_in|
    end for
    Select optimal location n* = arg max_n |K_in|
    Set optimal altitude h_i^* for location n*
    Sort MUs j ∈ K_in* by bandwidth requirement b_ij (ascending)
    while bandwidth B_i > 0 and FSO capacity not exceeded do
        Allocate b_ij to next MU j
        Associate MU j to UAV i
        Update B_i ← B_i − b_ij
    end while
    Initialize step size δ = d_min
    while δ ≤ d_max do
        h_i^- = max(h_i^* − δ, h^min)
        h_i^+ = min(h_i^* + δ, h^max)
        Calculate metrics m(h_i^-), m(h_i^+), m(h_i^*)
        if m(h_i^+) > m(h_i^*) or m(h_i^-) > m(h_i^*) then
            δ ← δ + d_min
            Update h_i^* according to Eq. (37)
        end if
    end while
end for
```

connection, minimizing interruptions, and enhancing service continuity. It optimizes the 2D location, altitude, and resource allocation for all UAVs. The time complexity is $\mathcal{O}\left(|I|\left(|N||J|+|J|+\frac{h_{\max}-h_{\min}}{d_{\min}}\right)\right)$, where $|I|$ is the number of UAVs, $|N|$ is the number of candidate locations, and $|J|$ is the number of MUs. The space complexity is $\mathcal{O}\left(|I||N|+|J|\right)$.

C. Proposed Bandwidth Allocation Solution

Once the 2D position of UAV i-th is finalized, bandwidth must be allocated to each covered MU to meet their data rate requirements. The minimum bandwidth needed for an MU j is calculated using:

$$b_{ij} = \frac{r_{ij}}{\log(1+\frac{P_i 10^{\frac{-\eta_{ij}}{10}}}{N_0})}. \tag{38}$$

However, the total available bandwidth of UAV i(denoted as B_i) is limited, making it impossible to satisfy all MUs. To maximize the number of MUs that receive sufficient bandwidth, the UAV i prioritizes MUs with the lowest bandwidth requirements. The allocation follows these steps:

*1) **MU arrangement**:* Create an array by arranging all the MUs covered by the UAV i (i.e., $\forall j \in K_{in^*}$) in ascending order based on their bandwidth requirements(b_{ij}). Let j_0 be the first MU in the sorted array. Allocate b_{ij_0} units of bandwidth to MU j_0, associate it with UAV i (i.e., set $a_{ij_0}=1$), and update the remaining available bandwidth of UAV i as $B_i = B_i - b_{ij_0}$.

*2) **Incremental allocation**:* Continue selecting the next MU in the sorted list, allocate the required bandwidth, and associate the MU with the UAV i. This process repeats until all the MUs covered by UAV i are connected (i.e.,$\forall j \in K_{in^*}, c_{ij}=1$, or until UAV i no longer has sufficient bandwidth to allocate to the next MU, or when the total data rate between the associated MUs and UAV i exceeds the capacity of the backhaul link FSO between UAV i and the OIRS in the building (constraint C5 in problem **P0**. The memory requirements for the MUs movement matrix and the MUs information matrix [29].

D. Traffic-Load Aware (TLA) Bandwidth Allocation

In the proposed OIRS-assisted mixed FSO/RF framework for UAVs-assisted temporary networks, this work compares our proposed bandwidth allocation algorithm with the traffic-load aware (TLA), to dynamically distribute backhaul capacity from the GS to four UAVs via segmented OIRS regions. The fundamental concept of TLA is to optimize the aggregate data rate between GSs and MUs by initially distributing bandwidth to MUs exhibiting reduced path loss to their corresponding GSs [29]. This ensures QoS provisioning for MUs in urban hotspots by prioritizing requests based on reliability/delay indices and waiting times $\rho_i = (r_i + d_i) \times \omega_i$, while ranking FSO channels using historical availability predictions $A_k = e^{-\alpha_k^p \times T_t^k} \times e^{-\alpha_k^s \times T_t^k}$ and EWMA-smoothed utility $U_{k,t} = (\sum U_{i,k}/N) \times \sigma + U_{k,t-1} \times (1-\sigma)$, yielding weights $W_k = A_k \times U_k$ that account for pointing misalignment, turbulence-induced fading, and overflow power interference. The OPT-UAV algorithm leverages this two-dimensional prioritization to jointly optimize UAVs positioning (x_u^i, y_u^i, h_i), user association (c_{ij}), and bandwidth allocation (r_{ij}), subject to backhaul constraints (C5), maximizing overall data rate Z while satisfying thresholds for availability and utility. Simulations demonstrate up to 25% enhancements in throughput and coverage over baselines, enabling resilient, scalable connectivity in blockage-prone environments.

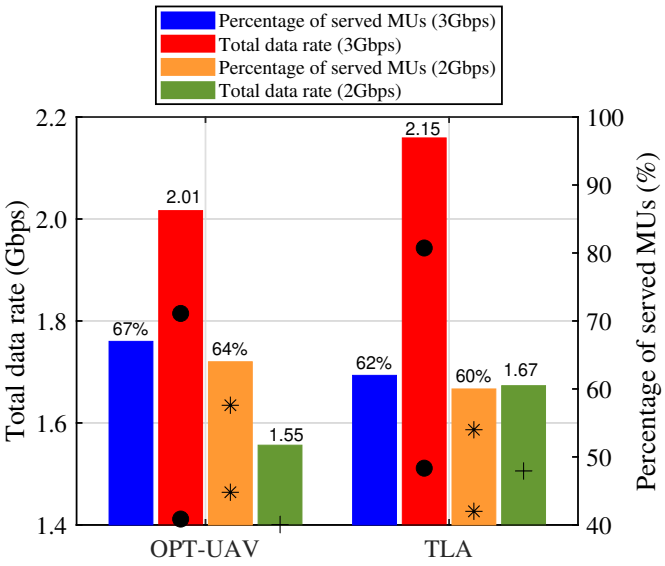

Fig. 4. Fraction of served MUs and total data rate incurred by different approaches.

TABLE II
SYSTEM PARAMETERS

Parameter	Symbol	Value
FSO transmission power	P_t	20 dBm
Divergence angle	θ_g	0.5 mrad
Receiver radius	r	0.05 m
Receiver sensitivity	N_b	67885 photons/bit
FSO wavelength	λ	1550 nm
Visible distance	v	5 km
Available UAVs		4
Disaster area radius		2 km
Maximum altitude of UAVs	$f^{\max}$	500 m
Carrier frequency	f_c	2 GHz
Environment index	b	9.61 [37]
Environment index	ζ	0.16 [37]
Average excessive pathloss in LoS	ξ_{LoS}	1 dB
Average excessive pathloss in NLoS	ξ_{NLoS}	20 dB
UAV downlink transmission power		20 dBm
Available bandwidth for each UAV	B_i	1 GHz

VI. NUMERICAL RESULTS

To assess the efficacy of our proposal, this study undertakes a comprehensive evaluation to compare its performance with baseline algorithms such as TLA. OPT-UAV and TLA utilize identical GS deployments, although they have distinct methodologies for allocating access link capacity. The numerical results presented in this study underscore the robustness and practicality of the proposed OIRS-enhanced FSO backhaul framework for UAVs-assisted irregular events, particularly in urban environments and disaster scenarios. By integrating OIRS with a mixed FSO/RF architecture, the system effec-

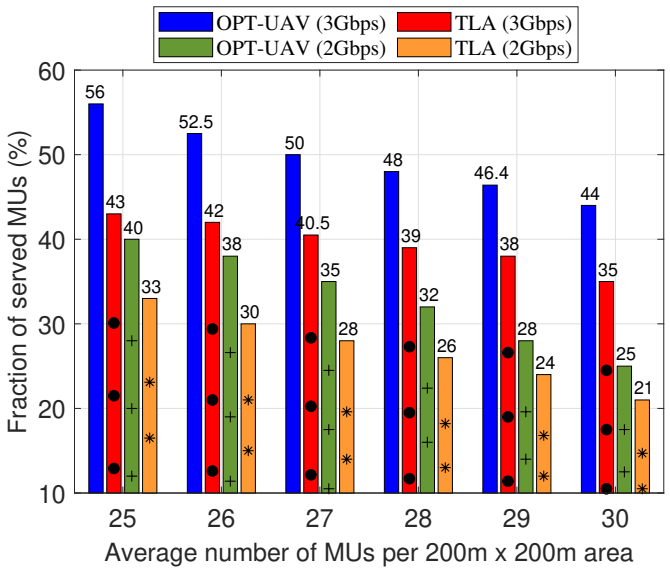

Fig. 5. Fraction of served MUs by varying the average MU density in the temporary zone

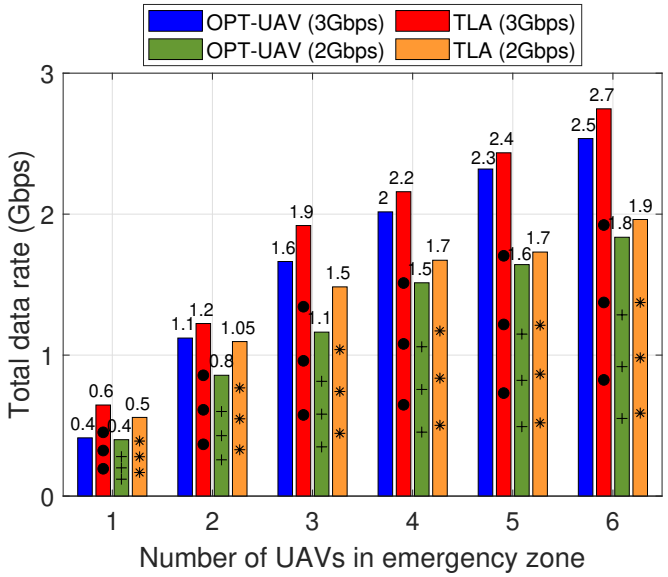

Fig. 6. Total data rate by varying the number of UAVs in the temporary zone

tively mitigates key challenges such as LOS blockages, atmospheric turbulence, and geometric misalignment, leading to enhanced link reliability and network scalability. The application of our proposed algorithm further improves the research's depth, as it provides a systematic and iterative approach to optimize UAVs placement, user association, and bandwidth allocation, ensuring QoS-aware resource management under constrained backhaul capacities. For a fair comparison, both the proposed OPT-UAV scheme and the TLA baseline are evaluated under identical simulation settings, including the same backhaul capacity, UAVs deployment scenarios, channel parameters, and QoS constraints. The key simulation parameters are summarized in Table **??**.

A core highlight of the results is the superior performance of our proposed algorithm in prioritizing user coverage and fairness, as evidenced in Fig. V-D. Here, our proposed approach achieves a 67% fraction of served MUs compared to 62% for the TLA method approach, albeit at a slightly lower total data rate (2.01 Gbps versus 2.15 Gbps with $R_i = 3$ Gbps). This outcome reflects the algorithm's strategic design: by sorting MUs based on ascending bandwidth requirements and iteratively allocating resources while respecting backhaul constraints (e.g., C5 in the optimization problem **P0**), our proposed algorithm maximizes the number of satisfied users without exceeding FSO capacities enhanced by OIRS. In contrast, TLA's focus on minimizing path loss for throughput maximization favors users with better channel conditions, potentially leaving more users underserved. This fairness-oriented mechanism in our proposed system is particularly valuable in temporary contexts, where equitable service distribution—rather than aggregate throughput—is critical for life-saving communications.

Next, the study is further illuminated by the sensitivity analyses in Figs. VI, which explores scalability under varying MUs densities and UAVs numbers. As average MUs density increases from 25 to 30 MU per $200\text{m} \times 200\text{m}$ location, the fraction of served MUs declines across both methods due to bandwidth limitations. However, our proposed consistently outperforms TLA (e.g., 56% versus 52.5% at density 25 MU with $R_i = 3$ Gbps), demonstrating its adaptability through altitude adjustments and dynamic re-association. This resilience stems from the algorithm's multi-stage process: initial 3D UAVs placement maximizes coverage via optimal elevation angles, followed by bandwidth allocation that enforces QoS thresholds (C4) and backhaul bottlenecks (C5). The integration of a comprehensive channel model—incorporating path loss, gamma-gamma turbulence fading, pointing error, and power interference—adds analytical rigor, allowing for to capture of real-world impairments like building vibrations and weather-dependent attenuation. OIRS plays a pivotal role here, as it stabilizes the FSO backhaul rate R_i by redirecting beams, effectively turning potential blockages into virtual LOS paths and boosting overall system performance.

Finally, Figs. VI and VI reveal the framework's scalability with increasing UAVs deployments. Total data rate rises monotonically with UAVs count (e.g., from 0.4 Gbps with 1 UAV to 2.5 Gbps with 6 UAVs under our proposed scheme with $R_i = 3$ Gbps), while served MUs fraction improves from 26% to 79% (Fig. VI). Although TLA yields higher throughput (e.g., 2.7 Gbps versus 2.5 Gbps at 6 UAVs), our proposed scheme's edge in coverage (79% vs. 73%) highlights its efficiency in resource-constrained scenarios. This is achieved through the algorithm's iterative altitude tuning (with step size δ in [dmin, dmax]) and periodic updates to adapt to MUs' mobility, ensuring compliance with altitude bounds (C2) and pathloss thresholds (C3). The OIRS enhancement indirectly amplifies these gains by improving R_i through reducing the effect of adverse issues, validating our contribution in linking backhaul reliability to downlink QoS.

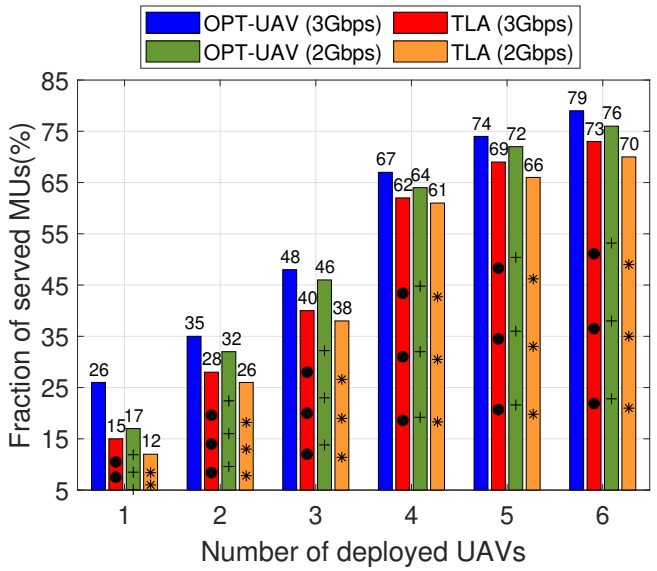

Fig. 7. Fraction of served MUs by varying the number of UAVs in the temporary zone

VII. Concluding Remarks and Future Works

This study proposed and evaluated an OIRS-enhanced FSO backhaul framework for UAVs-assisted mixed FSO/RF networks in dynamic urban and emergency scenarios. By integrating OIRS into UAVs-based FSO links, the system effectively addressed LOS blockages, turbulence, and misalignment, thereby creating virtual LOS paths and improving link stability. The proposed OPT-UAV algorithm jointly optimized UAVs placement, user association, and bandwidth allocation, ensuring QoS satisfaction under realistic channel impairments and constrained backhaul capacities. Numerical results highlighted significant improvements in user coverage and fairness over conventional approaches, validating the practicality of the proposed framework in temporary or disaster-driven environments.

Future endeavors will concentrate on improving flexibility and scalability via real-time OIRS phase control, multi-hop UAVs collaboration, and AI-driven traffic forecasting for anticipatory resource distribution. Specifically, integrating realistic OIRS flaws, including phase quantization errors and surface curvature constraints, into the channel model and optimization framework will be a crucial avenue for enhancing realism and resilience. These modifications are anticipated to enhance the function of OIRS-assisted mixed FSO/RF systems in developing robust and efficient next-generation wireless infrastructure.

Acknowledgement

This research is funded by Vietnam's Ministry of Information and Communications under Project DT.35/25.

References

[1] H. Kaushal and G. Kaddoum, "Optical communication in space: Challenges and mitigation techniques," *IEEE Communications Surveys & Tutorials*, vol. 19, no. 1, pp. 57–96, 2017. DOI:10.1109/COMST.2016.2603518.

[2] I. A. Alimi and P. P. Monteiro, "Revolutionizing free-space optics: A survey of enabling technologies, challenges, trends, and prospects of beyond 5g free-space optical (fso) communication systems," *Sensors*, vol. 24, no. 24, 2024. DOI:10.3390/s24248036.

[3] S. Hayat, E. Yanmaz, and R. Muzaffar, "Survey on unmanned aerial vehicle networks for civil applications: A communications viewpoint," *IEEE Communications Surveys & Tutorials*, vol. 18, no. 4, pp. 2624–2661, 2016. DOI:10.1109/COMST.2016.2560343.

[4] M. M. Azari, F. Rosas, K.-C. Chen, and S. Pollin, "Ultra reliable uav communication using altitude and cooperation diversity," *IEEE Transactions on Communications*, vol. 66, no. 1, pp. 330–344, 2018. DOI:10.1109/TCOMM.2017.2746105.

[5] L. Qu, G. Xu, Z. Zeng, N. Zhang, and Q. Zhang, "Uav-assisted rf/fso relay system for space-air-ground integrated network: A performance analysis," *IEEE Transactions on Wireless Communications*, vol. 21, no. 8, pp. 6211–6225, 2022. DOI:10.1109/TWC.2022.3147823.

[6] G. Xu, N. Zhang, M. Xu, Z. Xu, Q. Zhang, and Z. Song, "Outage probability and average ber of uav-assisted dual-hop fso communication with amplify-and-forward relaying," *IEEE Transactions on Vehicular Technology*, vol. 72, no. 7, pp. 8287–8302, 2023. DOI:10.1109/TVT.2023.3252822.

[7] V. Jamali, H. Ajam, M. Najafi, B. Schmauss, R. Schober, and H. V. Poor, "Intelligent reflecting surface assisted free-space optical communications," *IEEE Communications Magazine*, vol. 59, no. 10, pp. 57–63, 2021. DOI:10.1109/MCOM.001.2100406.

[8] Y. Xie, X.-Y. Liu, L. Kong, F. Wu, G. Chen, and A. V. Vasilakos, "Drone-based wireless relay using online tensor update," in *2016 IEEE 22nd International Conference on Parallel and Distributed Systems (ICPADS)*, pp. 48–55, 2016. DOI:10.1109/ICPADS.2016.0016.

[9] X. Sun and N. Ansari, "Latency aware drone base station placement in heterogeneous networks," in *GLOBECOM 2017 - 2017 IEEE Global Communications Conference*, pp. 1–6, 2017. DOI:10.1109/GLOCOM.2017.8254720.

[10] X. Sun and N. Ansari, "Jointly optimizing drone-mounted base station placement and user association in heterogeneous networks," in *2018 IEEE International Conference on Communications (ICC)*, pp. 1–6, 2018. DOI:10.1109/ICC.2018.8422377.

[11] R. I. Bor-Yaliniz, A. El-Keyi, and H. Yanikomeroglu, "Efficient 3-d placement of an aerial base station in next generation cellular networks," in *2016 IEEE International Conference on Communications (ICC)*, pp. 1–5, 2016. DOI:10.1109/ICC.2016.7510820.

[12] S. Zhang, X. Sun, and N. Ansari, "Placing multiple drone base stations in hotspots," in *2018 IEEE 39th Sarnoff Symposium*, pp. 1–6, 2018. DOI:10.1109/SARNOF.2018.8720492.

[13] M. Erdelj, E. Natalizio, K. R. Chowdhury, and I. F. Akyildiz, "Help from the sky: Leveraging uavs for disaster management," *IEEE Pervasive Computing*, vol. 16, no. 1, pp. 24–32, 2017. DOI:10.1109/MPRV.2017.11.

[14] S. ur Rahman, G.-H. Kim, Y.-Z. Cho, and A. Khan, "Positioning of uavs for throughput maximization in software-defined disaster area uav communication networks," *Journal of Communications and Networks*, vol. 20, no. 5, pp. 452–463, 2018. DOI:10.1109/JCN.2018.000070.

[15] A. M. Hayajneh, S. A. R. Zaidi, D. C. McLernon, M. Di Renzo, and M. Ghogho, "Performance analysis of uav enabled disaster recovery networks: A stochastic geometric framework based on cluster processes," *IEEE Access*, vol. 6, pp. 26215–26230, 2018. DOI:10.1109/ACCESS.2018.2835638.

[16] A. Chaaban, J. M. Morvan, and M. Alouini, "Free-space optical communications: Capacity bounds, approximations, and a new sphere-packing perspective," *IEEE Transactions on Communications*, vol. 64, pp. 1–1, 03 2016. DOI:10.1109/TCOMM.2016.2524569.

[17] Z. Zhao, Z. Zhang, J. Tan, Y. Liu, and J. Liu, "200 gb/s fso wdm communication system empowered by multiwavelength directly modulated tosa for 5g wireless networks," *IEEE Photonics Journal*, vol. 10, pp. 1–1, 06 2018. DOI:10.1109/JPHOT.2018.2851558.

[18] W. Fawaz, C. Abou-Rjeily, and C. Assi, "Uav-aided cooperation for fso communication systems," *IEEE Communications Magazine*, vol. 56, pp. 70–75, 01 2018. DOI:10.1109/MCOM.2017.1700320.

[19] M. Alzenad, M. Z. Shakir, H. Yanikomeroglu, and M.-S. Alouini, "Fso-based vertical backhaul/fronthaul framework for 5g+ wireless networks," *IEEE Communications Magazine*, vol. 56, no. 1, pp. 218–224, 2018. DOI:10.1109/MCOM.2017.1600735.

[20] Z. Gu, J. Zhang, Y. Ji, L. Bai, and X. Sun, "Network topology reconfiguration for fso-based fronthaul/backhaul in 5g+ wireless networks," *IEEE Access*, vol. 6, pp. 69426–69437, 2018. DOI:10.1109/ACCESS.2018.2880880.

[21] M. Najafi, H. Ajam, V. Jamali, P. D. Diamantoulakis, G. K. Karagiannidis, and R. Schober, "Statistical modeling of fso fronthaul channel for drone-based networks," in *2018 IEEE International Conference on Communications (ICC)*, pp. 1–7, 2018. DOI:10.1109/ICC.2018.8422552.

[22] H. Peng, Y. Zheng, P. He, Y. Cui, R. Wang, and D. Wu, "Reliability optimization in irs-assisted uav networks," *Vehicular Communications*, vol. 44, p. 100679, 2023. DOI:https://doi.org/10.1016/j.vehcom.2023.100679.

[23] S. Zhang, S. Gu, Y. Zhou, L. Shi, and H. Jin, "Energy efficient resource allocation of irs-assisted uav network," *Electronic Research Archive*, vol. 32, no. 7, pp. 4753–4771, 2024. DOI:10.3934/era.2024217.

[24] P. D. Pham, C. K. P. Nguyen, H. D. Le, H. T. T. Pham, T. V. Nguyen, and N. T. Dang, "Optical intelligent reflecting surface-assisted multiple users over turbulence channels," in *2024 RIVF International Conference on Computing and Communication Technologies (RIVF)*, pp. 45–50, 2024.

[25] H. Wang, Z. Zhang, B. Zhu, J. Dang, L. Wu, and Z. Gong, "Space division multiple access based on oirs in multi-user fso system," *IEEE Transactions on Vehicular Technology*, vol. 71, no. 12, pp. 13403–13408, 2022.

[26] A. Al-Hourani, K. Sithamparanathan, and S. Lardner, "Optimal lap altitude for maximum coverage," *IEEE Wireless Communications Letters*, vol. 3, pp. 569 – 572, 07 2014. DOI:10.1109/LWC.2014.2342736.

[27] L. Yu, X. Sun, S. Shao, Y. Chen, and R. Albelaihi, "Backhaul-aware drone base station placement and resource management for fso-based drone-assisted mobile networks," *IEEE Transactions on Network Science and Engineering*, vol. 10, pp. 1659–1668, 05 2023. DOI:10.1109/TNSE.2022.3233004.

[28] E. Kalantari and A. Yongacoglu, "On the number and 3d placement of drone base stations in wireless cellular networks," 04 2018. DOI:10.48550/arXiv.1804.08415.

[29] D. Wu, X. Sun, and N. Ansari, "An fso-based drone assisted mobile access network for emergency communications," *IEEE Transactions on Network Science and Engineering*, vol. PP, pp. 1–1, 09 2019. DOI:10.1109/TNSE.2019.2942266.

[30] M. R. Hayal, E. E. Elsayed, D. Kakati, M. Singh, A. Elfikky, A. I. Boghdady, A. Grover, S. Mehta, S. A. H. Mohsan, and I. Nurhidayat, "Modeling and investigation on the performance enhancement of hovering uav-based fso relay optical wireless communication systems under pointing errors and atmospheric turbulence effects," *Optical and Quantum Electronics*, vol. 55, May 2023. DOI:10.1007/s11082-023-04772-2.

[31] T. V. Nguyen, H. D. Le, N. T. Dang, and A. T. Pham, "Average transmission rate and outage performance of relay-assisted satellite hybrid FSO/RF systems," in *2021 International Conference on Advanced Technologies for Communications (ATC)*, pp. 1–6, 2021. DOI:10.1109/ATC52653.2021.9598287.

[32] M. A. Al-Habash, L. C. Andrews, and R. L. Phillips, "Mathematical model for the irradiance probability density function of a laser beam propagating through turbulent media," *Optical Engineering*, vol. 40, pp. 1554–1562, 2001.

[33] S. Shang, E. Zedini, and M.-S. Alouini, "Enhancing non-terrestrial network performance with free space optical links and intelligent reflecting surfaces," *IEEE Transactions on Wireless Communications*, vol. 24, no. 2, pp. 1046–1059, 2025. DOI:10.1109/TWC.2024.3504359.

[34] S. Shang, E. Zedini, A. Kammoun, and M.-S. Alouini, "A novel hybrid optical and star irs system for ntn communications," *IEEE Transactions on Wireless Communications*, pp. 1–1, 2025. DOI:10.1109/TWC.2025.3603722.

[35] E. E. Elsayed, "Performance enhancement in fso relay systems with miso via multi-hop m-ary ppm integrating and spatial modulation over gamma–gamma channels," *Journal of Optics*, vol. 54, pp. 3364–3379, 2025. DOI:10.1007/s12596-024-01936-5.

[36] H. Wang, Z. Zhang, B. Zhu, J. Dang, L. Wu, L. Wang, K. Zhang, Y. Zhang, and G. Y. Li, "Performance analysis of multi-branch reconfigurable intelligent surfaces-assisted optical wireless communication system in environment with obstacles," *IEEE Transactions on Vehicular Technology*, vol. 70, no. 10, pp. 9986–10001, 2021 DOI:10.1109/TVT.2021.3092722.

[37] W. Shi, J. Li, W. Xu, H. Zhou, N. Zhang, S. Zhang, and X. Shen, "Multiple drone-cell deployment analyses and optimization in drone assisted radio access networks," *IEEE Access*, vol. 6, pp. 12518–12529, 2018. DOI:10.1109/ACCESS.2018.2803788.